Colloquia: IFA 2010

Phase retrieval for X-ray in-line phase contrast imaging

F. Scattarella[1][2], S. Tangaro[2], C. Giannini[2][3], G. Gargano[2]
and R. Bellotti[1][2]

[1] *Dipartimento di Fisica "M. Merlin", Università di Bari - Bari, Italy*
[2] *INFN, Sezione di Bari - Bari, Italy*
[3] *IC-CNR - Bari, Italy*

Summary. — A review article about phase retrieval problem in X-ray phase contrast imaging is presented. A simple theoretical framework of Fresnel diffraction imaging by X-rays is introduced. A review of the most important methods for phase retrieval in free-propagation–based X-ray imaging and a new method developed by our collaboration are shown. The proposed algorithm, Combined Mixed Approach (CMA) is based on a mixed transfer function and transport of intensity approach, and it requires at most an initial approximate estimate of the average phase shift introduced by the object as prior knowledge. The accuracy with which this initial estimate is known determines the convergence speed of the algorithm. The new proposed algorithm is based on the retrieval of both the object phase and its complex conjugate. The results obtained by the algorithm on simulated data have shown that the obtained reconstructed phase maps are characterized by particularly low normalized mean square errors. The algorithm was also tested on noisy experimental phase contrast data, showing a good efficiency in recovering phase information and enhancing the visibility of details inside soft tissues.

PACS `42.30.-d` – Imaging and optical processing.
PACS `42.30.Rx` – Phase retrieval.
PACS `42.30.Va` – Image forming and processing.

1. – Introduction

Phase contrast X-ray imaging technique has attracted much interest in the scientific community in recent years. Conventional absorption-based imaging, where the contrast is generated by variations of the X-ray absorption coefficient that arise from density differences and from changes in thickness and composition of the sample. Phase contrast imaging derives contrast also from the phase modulations induced by the object onto the transmitted X-ray beam. These two effects can be described in terms of a complex index of refraction, which can be indicated as $n = 1 - \delta + i\beta$. The real part δ corresponds to the phase shift due to refraction and the imaginary part β to the absorption. Density

and composition differences of tissues influence the real part of the refraction index and change locally the X-ray wave speed, changing the wave phase, even in the absence of intensity wave attenuation. Moreover, for low-Z elements, phase shift cross sections are about 1000 times larger than the absorption ones, especially in the hard X-ray region, *i.e.*, at energies typical of radiography [1]. Consequently, phase contrast imaging (PCI) is possible also when absorption contrast is negligible. Another peculiarity is that phase contrast diminishes slower with energy with respect to absorption contrast. Therefore, it could also be used to decrease the dose delivered to patients.

Various methods for X-ray phase contrast imaging have been proposed and demonstrated, particularly over the last few years with the increasing use of synchrotron sources. Among all available X-ray PCI techniques, in-line PC Imaging (PCI) is the simplest experimental mode since no optics are required, a fundamental issue to transfer the results of laboratory research into hospitals.

A technique closely related to PCI is phase retrieval imaging (PRI). Indeed, PCI is an imaging modality thought to enhance the total contrast of the images, using the phase shift introduced by the object (*e.g.*, human body part) under investigation; PRI is a mathematical technique to extract the (quantitative) phase shift map from PCI [2,3]. The quantitative nature of PRI could open the possibility to access to essential information on the internal tissue/object structure, complementary to the attenuation-based imaging, obtained by conventional contact radiology.

Several are the mathematical algorithms which have been developed to retrieve quantitative information from PCI. A quantitative comparison between several phase retrieval algorithms in in-line PCI, based on the transport of intensity equation (TIE), on the contrast transfer function (CTF) and mixed TIE-CTF approaches (MAs), has been recently proposed in [4]. This work has shown that, although MAs [5-7] are slightly less computationally effective with respect to deterministic phase retrieval based on TIE/CTF, they lead to best performances in terms of quantitative results and robustness against noise.

In this work a new MA-based phase retrieval algorithm, called Combined Mixed Approach (CMA), is presented. In CMA algorithm the retrieved phase shift map is combined with its retrieved complex conjugate phase shift map [8]. The algorithm requires a very limited prior knowledge of the unknown phase, namely an initial approximate estimate of the average phase shift introduced by the object, that is always possible. The comparison of the results obtained by the new algorithm with other MA algorithms [5-7] on simulated data has shown. Moreover, the algorithm was also tested on poor-quality experimental PCI, obtaining a good efficiency in recovering phase information, also in the presence of very noisy data.

A simple theoretical framework is presented to treat Fresnel phase contrast diffraction imaging by X-rays. Then a review of the state of the art of the phase retrieval algorithm for the in-line phase contrast imaging is presented. Subsequently, the features of the new proposed algorithm and its application on simulated and real data are described.

2. – Fresnel phase contrast diffraction theory

The effect of the collective interaction of charges belonging to different atoms/molecules with an electromagnetic wave in a medium can be described by means of a refractive index n, related to the dielectric constant of the medium: $\epsilon = n^2$. The X-rays refractive index is defined by a real and an imaginary part: $n = 1 - \delta + i\beta$, the former related to elastic scatterings, the latter to inelastic ones [4], as said before. The absorption of the electromagnetic wave is described by the attenuation coefficient μ_t, that is related to the

absorption β by the following expression:

$$(1) \qquad \mu_t(x, y) = 2k \int_{\Delta z} \beta(x, y, z) \mathrm{d}z,$$

where $k = 2\pi/\lambda$, Δz is the thickness of the sample and (x, y, z) are the spatial coordinates of the sample. Moreover, the electromagnetic wave phase shift ϕ is related to the refractive decrement index δ by

$$(2) \qquad \phi(x, y) = -k \int_{\Delta z} \delta(x, y, z) \mathrm{d}z.$$

The propagation of electromagnetic waves is described by the wave equation that can be derived by Maxwell equations. For a quasi-monochromatic radiation/source we can write the wave equation as a solution of the well-known inhomogeneous *Helmotz equation* [9] in projection approximation:

$$(3) \qquad E_z(x, y) = E_0(x, y) T(x, y),$$

where $E_z(x, y)$ is the scattered wave out of the sample, $E_0(x, y)$ the incoming wave and $T(x, y)$ the *optical transmission function*, which describes the sample effects on the incident wave [9, 10]:

$$(4) \qquad \begin{aligned} T(x, y) &= \exp\left[-2k \int_{\Delta z} \beta(x, y, z) \mathrm{d}z + ik \int_{\Delta z} \delta(x, y, z) \mathrm{d}z\right] \\ &= A_0(x, y) \exp\left[i\phi(x, y)\right]. \end{aligned}$$

So, $T(x, y)$ shows the wave absorption and phase shift components introduced by the sample.

The free-space propagation of the outcoming wave from the object plane to the detector plane is described by the *Huygens-Fresnel principle*. The *Kirchhoff integral* solution in paraxial condition [9] defined the propagated wave function. In the so-called near-field Fresnel diffraction region, namely when the propagation distance is $z < R^2/\lambda$, where R^2/λ is the *Fresnel distance*, the *Kirchhoff integral* solution is

$$(5) \qquad E(x_1, y_1; z) = \frac{e^{ikz}}{i\lambda z} \int_{R^2} T(x_0, y_0) \exp\left[\frac{ik\left[(x_1 - x_0)^2 + (y_1 - y_0)^2\right]}{2z}\right] \mathrm{d}x_0 \mathrm{d}y_0,$$

where R^2 is the object surface and (x_1, y_1) and (x_0, y_0) are the object plane and the detector plane coordinates. The integral in eq. (5) is named *the Fresnel diffraction integral*. It is possible to observe that the integral in eq. (5) is of convolution type, which suggests Fourier transformation (FT) with respect to (x_1, y_1), giving

$$(6) \qquad \tilde{E}(u, v; z) = \exp[ikz] \tilde{T}(u, v) \exp\left[i\pi\lambda z(u^2 + v^2)\right],$$

where $\tilde{E}(u, v; z)$ and $\tilde{T}(u, v)$ are the wave equation and the transmission function in the Fourier domain, respectively. The z dependence is explicitly retained. The variables u and v represent spatial frequencies at the object or the image plane. The function

$\exp[i\pi\lambda z(u^2 + v^2)]$ is effectively the optical transfer function for Fresnel diffraction and may also be thought of as a *linear filter* acting on the transmitted frequencies. It is the FT of the so-called *Fresnel Propagator* (P_F).

After an algebraic manipulation of eq. (6), the intensity distribution of the image in the spatial-frequency Fourier domain $\tilde{I}$ can be related to the FT of the object transmission function modulated by the P_F [11]:

$$(7) \qquad \tilde{I}_D(\mathbf{f}) = \int T\left(\mathbf{x} - \frac{\lambda D\mathbf{f}}{2}\right) T^*\left(\mathbf{x} + \frac{\lambda D\mathbf{f}}{2}\right) \exp\left[-i2\pi\mathbf{x}\cdot\mathbf{f}\right] d\mathbf{x},$$

where $\mathbf{f} = (u, v)$ and $\mathbf{x} = (x, y)$ the Fourier coordinates and the real space coordinates, D is the de-focus distance that takes into account the distances between the source and the object z_1 and between the object and the detector z_2 ($D = z_1 z_2/(z_1 + z_2)$). It is important to underline that in the Fresnel phase contrast region, the object pattern is preserved and it is possible to recognize the edge enhancement effect. This effect is due to the dependence of the intensity pattern on the phase shift. In fact, in this case it is possible to prove [2] that $I \propto \nabla^2\phi$, where ϕ is the wave phase shift introduced by the object.

3. – Phase retrieval methods: state of the art

Phase retrieval problem is related to the problem of the phase information loss, that occurs when physical measurements are performed. In fact, an X-ray diffraction pattern is only a measurement of the intensity of the X-ray beam, that is mathematically the wave function absolute square. The phase retrieval problem arises in these applications in which wave phase is apparently lost or impractical to measure and only intensity data are available. Since the phase shift is proportional to proportional to the z-projected charge density of the object (see eq. (2)), once the phase map is retrieved, the refractive index can be reconstructed.

Different phase retrieval algorithms are available at the state of the art; they depend on both the characteristics of the sample (periodic/non-periodic), the diffraction regime (near-field/far-field) and the experimental set-up (with focusing optics/without focusing optics). A generic problem of phase retrieval in the Fresnel region can be stated as that of solving the following non-linear integral equation with respect to $\phi(x, y)$:

$$(8) \qquad \left|\mathbf{Fr}(A; \phi; k; \lambda; z)\right|^2 = I_z(x, y),$$

where $\mathbf{Fr}(A; \phi; k; \lambda; z)$ is the Fresnel integral in eq. (5), in which the dependence of $T(x, y)$ on the phase shift $\phi(x, y)$ is made explicit. For in-line free-propagation phase contrast in Fresnel regime, we have four main algorithms at the state of the art:

– Contrast Transfer Function (CTF) method [12],

– Transport of Intensity Equation (TIE) method [13],

– Weak Transport of Intensity Equation (WTIE) method [14],

– Mixed Approach (MA) method, that is CTF+TIE [7, 4, 6].

3˙1. *CTF*. – The method is based on the assumption of weak absorption and slowly varying phase shift. Starting from eq. (7), in these conditions it is possible to expand the transfer function $T(x,y)$ to the first order, so that the phase map is retrieved through the following expression:

(9)
$$\tilde{\phi}(\mathbf{f}) = \frac{1}{2\Delta + \alpha}\left[C\sum_D \tilde{I}_D \sin(\pi\lambda D\mathbf{f}^2) - A\sum_D \tilde{I}_D \cos(\pi\lambda D\mathbf{f}^2)\right],$$

$$A = \sum_D \sin(\pi\lambda D\mathbf{f}^2)\cos(\pi\lambda D\mathbf{f}^2),$$

$$B = \sum_D \sin^2(\pi\lambda D\mathbf{f}^2),$$

$$C = \sum_D \cos^2(\pi\lambda D\mathbf{f}^2),$$

$$\Delta = BC - A^2,$$

where the sum is made over different de-focus distances D (tipically 2-4 distances are used). α is a regularization term (Tikhonov regularization [15]).

3˙2. *TIE and WTIE*. – The methods are based on the assumption of short propagation distance. In this condition $T(\mathbf{x} \pm \frac{\lambda D\mathbf{f}}{2})$ can be expanded with respect to D and retaining only the first order. The result is the following expression, the so-called Transport Intensity Equation [16]:

(10)
$$\nabla\left[I_0(\mathbf{x})\nabla\phi(\mathbf{x})\right] = -\frac{2\pi}{\lambda}\frac{\partial I_0(\mathbf{x})}{\partial z},$$

with $I_0(\mathbf{x})$ is the attenuation intensity map at $D = 0$. In order to retrieve the phase shift map, the differential equation (10) can be solved using Fourier filters. The WTIE method is a variant of TIE method, which permits to retrieve the phase shift map assuming a weak absorbing object.

3˙3. *MA*. – MA method is based on the following two basic points:

1) a first estimate of the phase is derived from the difference map, obtained from at least two measures at different defocus distances (*e.g.*, a contact radiography I_0 at $D = 0$, and a PCI I_D for $D \neq 0$);

2) an iterative algorithm is applied: the phase retrieved is updated at the $(n+1)$-th cycle by means of a perturbation term which is applied to the phase retrieved at the n-th cycle.

The conditions of applicability of these methods are defined starting from CTF and TIE methods. The TIE is efficient in calculations and data, requiring images in two planes, but it is only valid for short propagation distances where the contrast is weak. The CTF, on the other hand, is only valid for weak absorption and slowly varying phase shift; so it is possible to combine the two methods assuming a slowly varying absorption and a slowly varying phase, so that when $D \rightarrow 0$ [7], TIE and CTF models approach the same expression. Therefore, if $|A(\mathbf{x} + \lambda D\mathbf{f}/2) - A(\mathbf{x} - \lambda D\mathbf{f}/2)| \ll 1$ and

$|\phi(\mathbf{x} + \lambda D\mathbf{f}/2) - \phi(\mathbf{x} - \lambda D\mathbf{f}/2)| \ll 1$, it is possible to linearize eq. (7) to obtain the following expression:

$$(11) \qquad \tilde{I}_D(\mathbf{f}) = \tilde{I}_D^{\phi=0}(\mathbf{f}) + 2\sin(\pi\lambda D\mathbf{f}^2)\mathcal{F}\{I_0\phi\} + iD\lambda\cos(\pi\lambda D\mathbf{f}^2)\mathbf{f}\cdot\mathcal{F}\{\phi\nabla I_0\},$$

with $\tilde{I}_D^{\phi=0}$ is the FT of the intensity at the distance D if the phase was zero. It can be approximated by $\tilde{I}_0$, that is the FT of the attenuation map (at $D = 0$). The perturbation term is proportional to the so-called phase-space shearing length $\lambda D|\mathbf{f}|$ [17]. The algorithm can be simply expressed in the Fourier domain of the spatial frequencies:

$$(12) \qquad \mathcal{F}[I_0\phi_{n+1}] = \frac{\tilde{I}_D(\mathbf{f}) - \tilde{I}_D^{\phi=0}(\mathbf{f}) + i\lambda D\cos(\pi\lambda D\mathbf{f}^2)\mathbf{f}\cdot\mathcal{F}[\phi_n\nabla I_0]}{2\sin(\pi\lambda D\mathbf{f}^2)},$$

where $\phi(\mathbf{x})$ map is calculated after 3-5 iterations. This formula has a phase regularization problem, related to those spatial frequencies for which the denominator goes to zero as well as in the use of prior information regarding the phase to be retrieved.

4. – The CMA algorithm

Starting from the above consideration we developed a new MA algorithm using $\langle\phi_{\text{prior}}\rangle$ as prior information and taking into account the mathematical property that relates the j-th derivative of the FT of a function to its moment of j-th order. In fact, for $j = 0$ it is known that for any function $g(\mathbf{x})$, in the origin of the Fourier domain ($\mathbf{f} = 0$) we find the mean value of g:

$$(13) \qquad \langle g\rangle = \int e^{-2i\pi\mathbf{x}\cdot\mathbf{f}}g(\mathbf{x})\,\mathrm{d}\mathbf{x}\bigg|_{\mathbf{f}=0}.$$

The phase shift introduced in the incident X-ray beam (of unitary intensity) can be obtained by the measured contact absorption image I_0, assuming that the object is homogeneous in composition with a constant δ/β ratio and using the Beer-Lambert law of absorption [18]:

$$(14) \qquad \phi_{\text{prior}} = \frac{\delta}{2\beta}\ln I_0,$$

where δ is the decrement of the complex refractive index, β is its imaginary part. The choice of the mean value of the phase shift as prior information is justified by its stability against the noise and the inhomogeneity of the illuminated sample.

With the CMA algorithm we wanted to reduce the error associated with the retrieved map respect the previous methods. For this purpose, we can retrieve the real phase shift and combine it with its conjugate, the latter retrieved solving the following equation [8]:

$$(15) \qquad \tilde{I}_D(\mathbf{f}) = \int e^{-2i\pi\mathbf{x}\cdot\mathbf{f}}T^*\left(\mathbf{x} - \frac{D\lambda\mathbf{f}}{2}\right)T\left(\mathbf{x} + \frac{D\lambda\mathbf{f}}{2}\right)\mathrm{d}\mathbf{x}.$$

Following the analogous derivation used to obtain eq. (12), we would obtain

$$(16) \qquad \mathcal{F}[I_0\phi_{n+1}] = \frac{\tilde{I}_D(\mathbf{f}) - \tilde{I}_D^{\phi=0}(\mathbf{f}) - i\lambda D\cos(\pi\lambda D\mathbf{f}^2)\mathbf{f}\cdot\mathcal{F}[\phi_n\nabla I_0]}{-2\sin(\pi\lambda D\mathbf{f}^2)},$$
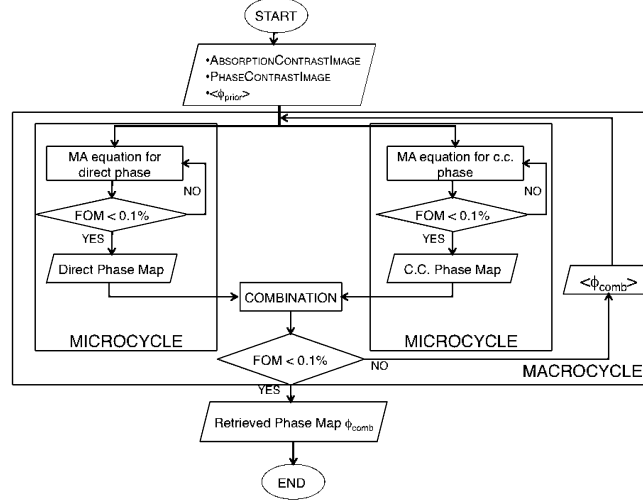
Fig. 1. – Flow chart of the CMA algorithm. A suitable FOM (figure of merit) stops automatically the microcycles and the macrocycles when the variation of the retrieved maps (ϕ, ϕ' or ϕ_{comb}) from a cycle n-th to the following $(n + 1)$-th is smaller than a suitable threshold (0.1%).

converging towards the complex conjugate of the object transmittance function. After some cycles, therefore, the iterative equation (16) will converge to a $\phi'_n = -\phi_{\mathrm{true}} + \Delta\phi'$, with ϕ_{true} the true phase to be retrieved changed in sign and $\Delta\phi'$ a residual phase error, irrecoverable through further application of the algorithm. Actually $\Delta\phi'$ will have opposite sign with respect to $\Delta\phi$ and, consequently, by combining the results of the two phase retrievals obtained by eqs. (12) and (16), a final phase retrieved value can be obtained:

$$(17) \qquad \phi_{\mathrm{comb}} = \frac{(\phi_n - \phi'_n)}{2} = \phi_{\mathrm{true}} + \Delta\phi_{\mathrm{comb}},$$

with $\Delta\phi_{\mathrm{comb}}$ in absolute value smaller than $|\Delta\phi|$ and $|\Delta\phi'|$.

The new proposed phasing algorithm is constituted by a macrocycle (that could be repeated, if needed) to retrieve the phase of $T(\mathbf{x})$, through the recursive equation (12) and of its complex conjugate through eq. (16), which are finally combined by means of eq. (17), as schematically shown in the flow chart of fig. 1. Moreover, instead of using a regularization parameter for the low frequencies, we will use the mean estimated phase obtained by eq. (14).

5. – The CMA applications on simulated and real data

The CMA iterative algorithm was tested using simulated images of a "virtual sample". The simulation was implemented by calculating the paraxial Fresnel-Kirchhoff diffraction integral directly [8]. For simplicity, an ideal pointlike monochromatic X-ray source and an ideal detector were assumed. The main parameters used for the simulated source and detector are

– X-ray energy $E = 20\,\mathrm{keV}$;

– source-object distance $z_1 = 2000\,\mathrm{cm}$;

– object-detector distance $z_2 = 200$ cm;

– defocus distance $D = 182$ cm;

– ideal detector pixel pitch $= 50 \, \mu$m;

– images size $= 330 \times 330$ pixels.

– magnification factor $M = 1.1$.

To test the quantitativeness of the algorithm, we used a sample with distinct distributions (images) of both attenuation and phase maps without noise. The virtual object transmittance function has been calculated starting from these simulated distribution. The simulated PCI has been obtained applying eq. (5) to the obtained object transmittance function. So, we have used the simulated PCI and the simulated attenuation image as the only two input maps of the CMA. The convergence of the CMA depends on the input prior estimation: when we start by $\langle \phi_{\mathrm{prior}} \rangle$, only one macrocycle, constituted by three microcycles for phase retrieved map and for complex conjugate phase retreived map each, is needed; when the prior information is not used, we reach the same result but the convergenge is very slow (about fifteen microcycles are needed). For simulated images the reconstruction of the phase map can be compared directly with the input phase map, denoted as ϕ_{true}. In this case it is possible to define the NMSE (Normalized Mean Square Error) expressed as a percentage:

$$(18) \qquad \mathrm{NMSE} = 100 \times \sqrt{\frac{\sum |\phi_{\mathrm{true}}(x) - \phi(x)|^2}{\sum |\phi_{\mathrm{true}}(x)|^2}} \, .$$

The NMSE values obtained for the retrieved phase $\phi(x)$ and for its complex conjugate are, respectively, of 24% and 22%. Let us note this error metric can be both affected by any arbitrary additive constants that may be present in the retrieved phase, by regularization problems and by incorrect numerical evaluations of the intensity gradients, present in the perturbation term of eq. (12) and eq. (16), which are iteratively updated during the phase retrieval process. We have obtained similar NMSE values starting from the attenuation and phase maps described before and implementing the algorithms of [6,8,9]. The combination of the two retrieved phases leads to a final NMSE $= 7.2\%$, only one third of that obtained without the combination with the complex conjugate phase retrieval. A comparison between this value with the results of the previous algorithm is shown in table I.

In order to verify these findings from an experimental point of view, we applied the CMA algorithm to experimental attenuation and phase contrast images of a sample consisting in a grid of 6×6 nylon wires of different diameters nominally from 0.1 to 0.6 mm. The images were taken at the SYRMEP beam-line of ELETTRA [19]. We used poor-quality experimental phase contrast data, characterized by Peak-to-Peak Signal-to-Noise

TABLE I. – *NMSE values for different phase retrieval algorithms* [4,8].

Methods	NMSE
TIE, WTIE, CTF, MA	22–24%
CMA	7.2%

Ratio (PPSNR) ranging between 3 and 7 dBs for attenuation image and between 13 and 15 dBs for PCI, in order to deal with quite noisy data. The main experimental parameters are here summarized:

– X-ray energy $E = 20\,\mathrm{keV}$;

– source-object distance $z_1 = 2300\,\mathrm{cm}$;

– object-detector distance $z_2 = 173.5\,\mathrm{cm}$;

– exposure times down to $1\,\mathrm{s}$;

– detector pixel pitch $= 4.5\,\mu\mathrm{m}$;

– images size $= 760 \times 760$ pixels.

The retrieved phase map have been obtained after three macrocycles, each composed of six microcycles (three for the phase retrieval and three for the conjugate phase retrieval). For the experimental data, ideal reconstructions are not available and only theoretical values of the refractive index are known. So, it has been possible to evaluate an Average Normalized Error (AVGE) [4] between the retrieved δ_{ret}, obtained from the phase retrieved map using eq. (2) averaging the results along the fiber axis, and the theoretical value δ_{th}:

$$(19) \qquad \mathrm{AVGE} = 100 \times \frac{(\delta_{\mathrm{ret}} - \delta_{\mathrm{th}})}{\delta_{\mathrm{th}}} \,.$$

We found that within a 3% AVGE error, there is a good quantitative agreement between nominal value of δ_{th} for *nylon 6,12* (8 C diamine and 12 C diacid) and the experimental retrieved results. The new proposed algorithm has shown a good efficiency in recovering phase information also for noisy data on weakly absorbing objects (nylon wires). This experiment has confirmed that the smaller the feature to imaged, the larger the gain in visibility of PCI *versus* ACI, whenever the detector resolution does not limit its visibility. Moreover, it has been shown how this visibility can be further enhanced via PRI. In fact PRI is characterized by lower level noise than PCI or ACI. In order to study the visibility of different images (attenuation-based, PCI, retrieved phase-map), one can calculate the Contrast to Noise Ratio (CNR) defined by

$$(20) \qquad \mathrm{CNR} = \frac{|\langle I_{\mathrm{ob}} \rangle - \langle I_{\mathrm{bk}} \rangle|}{\sqrt{\sigma_{\mathrm{ob}}^2 + \sigma_{\mathrm{bk}}^2}} \,.$$

Here $\langle I_{\mathrm{ob}} \rangle$ and $\langle I_{\mathrm{bk}} \rangle$ are the mean intensity values of a given area in the object (wires) and the background (air), respectively; σ_{ob}^2 and σ_{bk}^2 the respective standard deviations. In fig. 2 the PCI/ACI contrast to noise ratio and the PRI/ACI contrast to noise ratio *versus* the fiber size of the nylon wires sample have been plotted. As discussed in ref. [10], the presented experiment confirmed that the smaller is the feature to be imaged, the larger is the gain in the visibility of PCI *vs.* ACI, whenever the detector resolution does not limit its visibility. This is demonstrated by the red line in fig. 2. Here it is also shown that the visibility can be further enhanced via PRI (blue line). Indeed, although PCI is characterized by an edge enhancement (see fig. 5 in ref. [8]), which is lost in the PRI map, the latter is characterized by better CNRs compared to both the
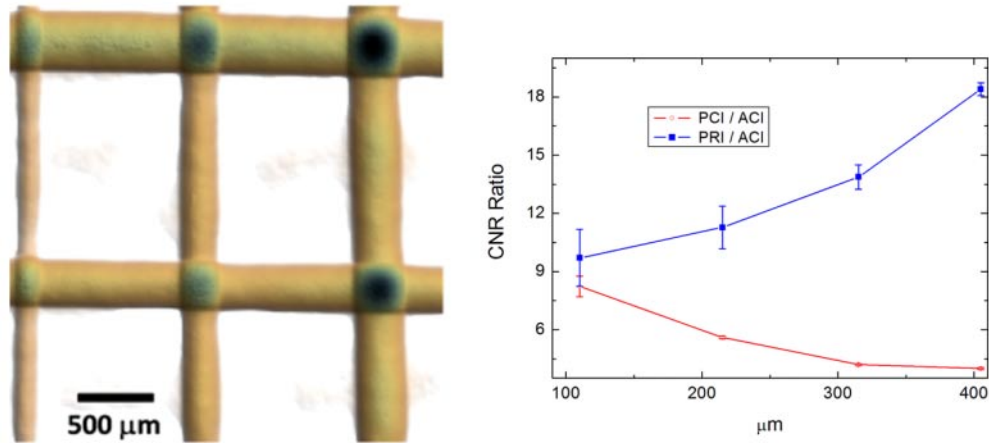
Fig. 2. – (Colour on-line) Retrieved phase map (left) of a region of the sample obtained by the proposed algorithm [8]. The ratio of PCI-CNR to the ACI-CNR (red line) and the ratio of PRI-CNR to the ACI-CNR (blue line) are shown *vs.* the fiber size (right).

attenuation and the PCI maps. We can conclude that PRI can be used not only to have quantitative phase-shift maps, leading essential information on the internal structures of soft tissues complementary to attenuation information, but it could be used also the enhance visibility of details inside soft tissues.

6. – Conclusion

For clinical X-ray imaging, such as mammography, small differences are expected between the phase contrast image and the attenuation image. With the help of phase retrieval it could be possible to retrieve phase information to enhance the visibility of the structures and to access to quantitative information of the sample, such as its internal composition. It is important also to take into consideration that the noise level could also be strongly enhanced in the different image (PCI minus ACI) used for phase retrieval. Therefore, very robust phasing algorithms against noise are needed in order to realize qualitative/quantitative PRI of human body parts. To verify these potentialities of PRI, we are planning suitable phase contrast experiments on samples with a structured background to study the noise effects on these imaging technique. Moreover, we are also planning volumetric-CT phase contrast experiments, as one of the main interests of PRI is just 3D tomographic imaging [17]. Non iterative phase retrieval algorithms for volumetric-CT phase contrast imaging will be studied. Finally, the influence of the detector resolution and the source size on the phase contrast images can be important to retrieve correct phase maps. In [20], it has been shown that also very simple deconvolution procedures could bring significant improvements in phase contrast images, which are substantially degraded by convolutions with detector resolution. A similar effect is possible when excessive source sizes or higher-resolution detector, with a point spread function comparable to the source distribution, are used in phase contrast imaging. We are planning more sophisticated deconvolution procedures that might remove at least in part the negative effects of the source size from the acquired images. These procedures could make phase retrieval more efficient.

REFERENCES

[1] SAYRE D. and CHAPMAN H. N., *Acta Crystallogr. A*, **51** (1995) 237.
[2] POGANY A., GAO D. and WILKINS S. W., *Rev. Sci. Instrum.*, **68** (1997) 2774.
[3] DAVIS T. J., GAO D., GUREYEV T. E., STEVENSON A. W. and WILKINS S. W., *Nature*, **373** (1995) 595.
[4] LANGER M., CLOETENS P., GUIGAY J. P. and PEYRIN F., *Med. Phys.*, **35** (2008) 4556.
[5] WU X. and LIU H., *J. X-Ray Sci. Technol*, **11** (2003) 33.
[6] MENG F., LIU H. and WU X., *Opt. Express*, **15** (2007) 8383.
[7] GUIGAY J. P., LANGER M., BOISTEL R. and CLOETENS P., *Opt. Lett.*, **32** (2007) 1617.
[8] DE CARO L., SCATTARELLA F., GIANNINI C., TANGARO S., RIGON L., LONGO R. and BELLOTTI R., *Med. Phys.*, **37** (2010) 3817.
[9] BORN M. and WOLF E., *Principle of Optics* (Cambridge University Press, Cambridge) 1997.
[10] DE CARO L., GIANNINI C., CEDOLA A., BUKREEVA I. and LAGOMARSINO S., *Phys. Med. Biol.*, **53** (2008) 6619.
[11] GUIGAY J. P., *Optik*, **46** (1977) 121.
[12] CLOETENS P. *et al.*, *Appl. Phys. Lett.*, **75** (1999) 2912.
[13] NUGENT K., GUREYEV T., COOKSON D., PAGANIN and BARNEA Z., *Phys. Rev. Lett.*, **77** (1996) 2961.
[14] BRONNIKOV A. V., *J. Opt. Soc. Am. A*, **19** (2002) 472.
[15] TIKHONOV A. N. and ARSENIN V. A., *Solution of Ill-Posed Problems* (Winston & Sons, New York) 1977.
[16] TEAGUE M. R., *J. Opt. Soc. Am.*, **72** (1982) 1199.
[17] WU X., LIU H. and YAN A., *Eur. J. Radiol.*, **68** (2008) S8.
[18] PAGANIN D. M., *Coherent X-ray Optics* (Oxford University Press, New York) 2006.
[19] ABRAMI A. *et al.*, *Nucl. Instrum. Methods Phys. Res. A*, **548** (2005) 221.
[20] OLIVO A. and SPELLER R. D., *Phys. Med. Biol.*, **54** (2009) N347.